The Measurement of the Intrinsic Impurities of Molybdenum and Carbon in the Alcator C-Mod Tokamak Plasma using Low Resolution Spectroscopy.

M. J. May, M. Finkenthal[*], S. P. Regan, and H. W. Moos
Plasma Spectroscopy Group
The Department of Physics and Astronomy
The Johns Hopkins University, Baltimore MD.

J. L. Terry, J. A. Goetz, M. A. Graf, J. E. Rice, and E. S. Marmar
Plasma Fusion Center
Massachusetts Institute of Technology, Cambridge MA.

K. B. Fournier[†] and W. H. Goldstein
Lawrence Livermore National Laboratories

---

[*] Racah Institute of Physics, Hebrew University, Jerusalem, Israel.

[†] Department of Physics and Astronomy, The Johns Hopkins University.

Abstract:

The intrinsic impurity content of molybdenum and carbon was measured in the Alcator C-Mod Tokamak using low resolution, multilayer mirror (MLM) spectroscopy ($\Delta\lambda \sim 1 - 10$ Å). Molybdenum was the dominant high-Z impurity and originated from the molybdenum armor tiles covering all of C-Mod's plasma facing surfaces (including the inner column, the poloidal divertor plates, and the ICRF limiter). Despite the all metal first wall, a carbon concentration of 1 - 2 % existed in the plasma and was the major low-Z impurity in Alcator C-Mod Tokamak. Thus, the behavior of intrinsic molybdenum and carbon penetrating into the main plasma and the effect on the plasma must be measured and characterized during various modes of Alcator C-Mod Tokamak operation. To this end, strong XUV emission lines of charge states ranging from H like through He like lines of carbon (radius/minor radius, r/a ~1) at the plasma edge to K through Cl like ($0.4 < r/a < 0.6$) and Mg through Na like ($r/a < 0.4$) of molybdenum in the main plasma were measured using a novel, low resolution, photometrically calibrated polychromator with MLMs as dispersive elements. The MLM spectra were investigated in detail, and comparisons with high resolution spectroscopy were made. The utility of the low resolution spectroscopy to diagnose tokamak plasmas is presented, and meaningful information about impurity behavior was obtainable due to the specific choice of the observed spectral regions. *Ab initio* physics rates from the HULLAC atomic physics package were input into the collisional radiative model and the MIST, and both were used in the interpretation of

the molybdenum spectrum. The carbon spectrum was interpreted using the MIST particle transport code and the direct impact rates of Itikawa that were incorporated into the collisional radiative model. The intrinsic ion concentrations, their contribution to the Z_{eff} -1, and power losses through line radiation were estimated. For the diverted ohmically heated plasma examined in this paper, the intrinsic molybdenum and carbon concentrations in the core plasma were found to be ~1.2×10^{10} cm^{-3} and ~1.7×10^{12} cm^{-3}, respectively. These measurements were obtained before the plasma facing components were boronized. The calculated radiation from molybdenum was 170 kW; for carbon this was 45 kW. The contribution to the measured Z_{eff} -1 of ~0.8 was ~0.11 for molybdenum and ~0.5 for carbon.

Introduction:

The concentration of impurities in the plasma and their radiated power through line emission inside the radius of the limiter or the magnetic separatrix are of great concern for tokamak fusion physics devices. These measurements typically have been performed using large vacuum ultraviolet (VUV) and soft X-ray extreme ultraviolet (XUV) normal and grazing incidence grating spectrometers. Unfortunately, the physical access and the direct views of both the main plasma and the divertor regions that are required by these diagnostics will be severely limited due to radiation shielding and vessel cooling hardware in future tokamaks. These constraints may prohibit the use of such systems in future fusion physics devices. Alternatively, fiber optics coupled to visible spectrometers located far from the tokamak provide a method for observing spectral line emission. However, unlike the UV transitions, a visible transition does not directly relate to the ground state of the emitting charge state. The inferred ground state densities from the visible transitions will be highly model dependent. An attractive alternative to both these conventional spectroscopic systems is the low resolution multilayer mirror (MLM)-based polychromator [1,2]. MLM-based systems are simple, high-throughput, compact XUV devices with fast time response. A prototype, three channel, MLM-based polychromator has been installed on the Alcator C-Mod Tokamak to examine the utility of the MLM-based diagnostic for tokamak impurity measurements and more specifically to monitor the brightness of the resonant XUV emission lines of carbon and molybdenum from the main plasma. From these

spectroscopic measurements, the intrinsic impurity transport information, impurity concentration and the radiative power losses were determined for an ohmically heated plasma operated in a diverted configuration. For the most part, these impurity measurements can be made without the need for conventional high resolution systems. The low resolution multilayer mirror based systems can do the job.

The molybdenum content in the Alcator C-Mod Tokamak plasma was of great concern because the interior armor tiles, ICRF limiter and, poloidal divertor plates were machined molybdenum blocks. At the central electron temperatures of 1 - 4 keV in Alcator C-Mod, molybdenum (Z = 42) existed as Mo^{30+} to Mo^{33+} ions in the plasma center. Therefore, molybdenum radiated strongly throughout the plasma. This molybdenum radiation could cause problems in attaining the highest performing plasmas since fusion plasmas can tolerate only a very small amount of high-Z impurities for break-even conditions [3].

The presence of carbon in the C-Mod plasma was also a concern. The significant amount (1 - 2% of the electron density) of carbon in the machine was unexpected due to the all molybdenum first wall. The measured concentration of carbon was a significant contribution to the Z_{eff} -1 and was similar to that seen in the DIII-D Tokamak [4]. Fortunately, the plasma can tolerate a larger amount of low-Z impurities because carbon was fully ionized in the plasma core and only radiates near ($0.8 < r/a < 1.0$) the last closed flux surface (LCFS).

Experiment:

In the experiments described in this paper, the Alcator C-Mod Tokamak had a plasma current, I_p, of 800 kA, a central electron density, n_{e0}, of 1.0 - 1.5x10^{14} cm^{-3}, and a central electron temperature, T_{e0}, of 1 - 4 keV in deuterium discharges (Table I). The central toroidal magnetic field, B_t, was 5.3 T. The Alcator C-Mod Tokamak had a major radius, R, of ~ 67 cm and a minor radius, a, of ~ 22 cm in either a limited or a magnetically diverted configuration. A cross section of a diverted plasma configuration is shown in Fig. 1. The electron temperature profile was measured from electron cyclotron emission (ECE) [5]. The electron density was measured using two color interferometry (TCI) [6]. The impurity particle transport parameters were determined using the trace impurity laser ablation method [7]. Each impurity injection, which introduced ~ 1x10^{17} particle into the plasma, had no discernible effect on the electron density. Therefore, these impurity injections did not cause significant perturbations to the plasma. The total power losses from the plasma were measured with a spatially resolving bolometer which was sensitive to photons from the visible through the x-ray (10 keV) and to energetic neutral particles [8]. The Z_{eff} measurements of the core plasma have been determined from visible bremsstrahlung emission [9]. Simultaneously with the MLM-based polychromator measurements, VUV spectra were obtained with a high resolution, 2.2 m, photometrically calibrated (to ±20%), grazing incidence spectrograph (GIS). The spectral resolution of the GIS was .5 to 1 Å. The 1^{st} order wavelength range was

60 to 1100 Å, with ~ 50 Å covered during each plasma. Typical integration times were 2 to 8 ms.

Our multilayer mirror (MLM)-based XUV polychromator obtained the low resolution spectral information of carbon and molybdenum. The instrument was photometrically calibrated to ± 20% from 10 - 140 Å. The MLM resolution, $\Delta\lambda$, was ~ 0.5 Å at 30 Å, ~ 2.5 Å at 75 Å and ~ 7 Å at 130 Å. The temporal resolution with the current emission brightness was ~ 1 ms. The polychromator had a fixed radial view chord through the center of the plasma (Fig. 1) and had a spatial resolution of ~ 1 cm. The MLM polychromator had two modes of operation. First, the time histories of three different wavelengths (λ = 127.9 Å, 74.9 Å, and 39.5 Å) were obtained simultaneously during the duration of the plasma. Second, the spectral information of the three regions was obtained simultaneously by scanning the wavelength of the polychromator during the steady state portion of a plasma. The instrument has been described in more detail elsewhere [10,11].

The Low Resolution MLM Spectra:

The utility and limitations of low resolution MLM spectroscopy needed to be addressed and understood thoroughly. The present experiments include a significant fraction of the usable spectral range of the MLMs and presents an excellent test of tokamak impurity physics analysis using low resolution spectroscopy. It is important to point out that the possibilities and limitations of the low resolution spectroscopy depend on the types of intrinsic impurities present in the plasma, the wavelengths of their specific atomic transitions, and the use of an adequate atomic physics model. Low-Z impurity emissions are typically strong resonance transitions due to their simple ion structure and, as a result, are well isolated from each other in wavelength. In contrast, ions of high-Z impurities emit photons in strong resonance transitions as well as in large bands of p-d transitions that are unresolvable even with high resolution spectrographs.

The wavelength region monitored by these low resolution MLM systems must exploit the specifics of the emitting trace impurities in the tokamak plasma so that meaningful spectra can be obtained. For the Alcator C-Mod Tokamak the MLM-based polychromator was configured to measure simultaneously specific emission regions of the carbon and molybdenum spectrum in the 30 - 40 Å, 60 - 85 Å, and 110 - 140 Å wavelength regions. In the 30 - 40 Å range the 3d - 4f Mo^{14+} to Mo^{15+} and 3d - 4p Mo^{15+} to Mo^{18+} transitions overlap with the dominant resonant carbon lines of C^{5+} at 33.7 Å (Lyman α) and C^{4+} at 40 Å. These molybdenum charge states existed near the plasma edge in very narrow

shells. The electron temperature was too low to excite these ions into the many upper levels that feed these transitions. Therefore, the molybdenum emission lines were seen as a weaker background under the carbon emission. To interpret the carbon impurities, a simple model of the few bright lines was all that was necessary. Between 60 - 85 Å, not only was the resolution lower than at 30 - 40 Å, but the molybdenum spectra became more complex. The Mo emission consisted of strong 3p - 3d lines and a 3p - 3d, quasi-continuum of unresolved lines. The challenge was to extract meaningful spectral information under this seemingly adverse situation. A thorough investigation and a detailed spectral model of the transition lines were necessary to understand fully the spectrum and to extract information about the impurities. Finally, the specifics of the molybdenum radiation patterns at 110 - 140 Å made the interpretation possible at the lowest resolution of the MLM. Only two lines of Mo^{30+} and Mo^{31+} emit strongly in this spectral region and only a simple spectral model was required. The interpretation was relatively easy as will be shown.

(a) The 110 - 140 Å Spectral Region of Molybdenum:

The low resolution of the MLM ($\Delta\lambda \sim 7$ Å) necessitated an experimental investigation of the emission in the 110 - 140 Å spectral region using the GIS. It was clear from the GIS spectrum (Fig. 2(c)) that the concentration of molybdenum was by far the largest of the high-Z impurities in the plasma. The spectra from the GIS had a background level which was assumed to be scattered light and not real XUV photons since it did not appear on the MLM spectrum. The background level was

subtracted and the final spectra is plotted in Fig. 2(c). The two strong and well-isolated emission lines in the spectrum were the Mo^{30+} (Mg like) $3s^2$ $^1S_0$ - 3s3p $^1P_1$ at 115.9 Å and Mo^{31+} (Na like) 3s $^2S_{1/2}$ - 3p $^2P_{3/2}$ resonant line at 127.9 Å [12]. These charge states emit in the central region of the plasma (r/a < 0.4) under the present experimental conditions. Spectral blending with emission lines of other impurities could be a significant problem with the low resolution of the MLM. If a significant concentration of iron would be present in the plasma, the strong $2s^2$ - 2s2p line at 132.9 Å of Fe^{22+} (Be like) would contaminate the MLM spectra. As seen in the GIS spectra in Fig. 2(c), iron was not present in the plasma. The major lines that could blend with the dominant molybdenum emission were the F^{5+} 2s2p - 2s3d line at 139.9 Å, the C^{5+} 2s-4p transition at 134.9 Å and a very weak Mo^{31+} 3p - 3d line at 134.6Å. These emission lines were not as bright as and were well separated in wavelength from the Mo^{30+} and Mo^{31+}. Therefore, the measured low resolution molybdenum spectral peaks should not be significantly blended with emission from carbon, iron, or fluorine.

To understand fully the low resolution MLM spectrum in the 110 - 140 Å region, the MLM spectral scan was analyzed in detail and then compared with that taken with the GIS. The uncalibrated MLM spectrum shown in Fig. 2(a) was taken during the steady state portion of an ohmically heated diverted discharge. The chi-squared, spectral line fit (thin solid curves, Fig. 2(b)) incorporated the instrumental line widths (Lorentzian) of the MLM polychromator and the known dominant lines of the molybdenum and carbon charge states in the region, to determine the intensity in volts of each emission line. The photometric calibration was

then applied to each fitted line. The good spectral fit in this region was possible due to the specifics of the emission; the spectrum was very simple and the emission lines were separated in wavelength by more than the bandpass of the multilayer. The spectral fit from the MLM agreed well with the measured brightness from the GIS (solid vertical lines) and had even a better agreement with the synthetic spectrum calculated by the collisional radiative model that is shown slightly offset in wavelength for clarity (dashed line - see Atomic Physics Model section). The uncertainties in the line brightnesses between the GIS and the MLM-based polychromator were within the uncertainties of the photometric calibrations of both instruments.

The time histories from the two instruments during the same plasma discharge are shown for the 127.9 Å Mo^{31+} line in Fig. 3. For this discharge the plasma was limited against the inner wall for the first 300 ms. The plasma was then diverted after 300 ms. At 700 - 1000 ms the dipole ICRF antennas were pulsed. In the second trace (dotted line), the GIS resolution was degraded to that of the MLM-based polychromator by a computer code using the Lorentzian instrumental line width of the MLM. This GIS trace (dotted line) included all the photons that the GIS would see if the GIS had the MLM spectral response. For direct comparison, the time histories of the MLM-based instrument (solid line) and the GIS (dotted line) were normalized at 700 ms to remove any photometric cross calibration errors. The agreement between the MLM and this GIS trace at each point in the discharge was excellent. The third trace (dashed line) included just the brightness of the 127.9 Å line measured with the GIS and agreed quite well with the other two traces. The contamination of the

MLM spectrum by emission other than the 127.9 Å line was less than 10% as expected after the examination of the GIS spectra in Fig. 2(c). Therefore, the majority of the emission seen by the MLM-based spectrometer was the strong resonant Mo^{31+} 127.9 Å line. A similar situation existed for the 115.9 Å emission line of Mo^{30+}. Despite the low resolution, a meaningful spectrum and time history were measured by the MLM-based polychromator. Therefore, on the Alcator C-Mod Tokamak the MLM spectra from 110 - 140 Å region could be used for impurity behavior analysis during different tokamak operating regimes without the need of a conventional GIS.

(b) The 65 - 80 Å Spectral Region of Molybdenum:

In the 65 - 80 Å region, the interpretation of the spectra was more difficult. Although, the resolution was significantly better ($\Delta\lambda \sim 2.5$ Å) the spectrum was more complex. Several strong 3p-3d transitions of Mo^{23+} to Mo^{25+} were the major line radiators [13,14,15] which were unresolvable by the MLM-based polychromator. These Mo^{23+} to Mo^{25+} charge states were characteristic of intermediate ionization states ($0.4 < r/a < 0.6$) in the C-Mod Tokamak plasma and were used for the main plasma impurity analysis in this spectral region. In addition, a large number of $3p^6 3d^k$ - $3p^5 3d^{k+1}$ transitions emitted from the Mo^{15+} - Mo^{22+} ionization states [16] exist as a background under the molybdenum K to Cl like lines. These ionization states had their maximum fractional abundance at an r/a greater than 0.8 and were characteristic of edge states. A synthetic

spectrum of these $3p^6 3d^k$ - $3p^5 3d^{k+1}$ transitions calculated *ab initio* is plotted in Fig. 4 with each line given the GIS spectral resolution.

The relative contribution of the quasi-continuum emission (Mo^{15+} - Mo^{22+}) to the line emission (Mo^{23+} to Mo^{25+}) in the low resolution spectrum needed to be determined and removed. Our purely experimental approach using the GIS was as follows. The time histories of both instruments were taken during the same plasma discharge (Fig. 5). The polychromator was centered at 74.9 Å (solid line). For this discharge the plasma was diverted after 300 ms. There was a trace molybdenum impurity ablation at ~ 400 ms. The input of ~1 MW of ICRF power from the dipole antenna caused the increase in the Mo emission between 500 - 800 ms. For the GIS, two time histories were created as described above for the Mo^{31+} 127.9 Å line and are presented for the spectrum centered at 74.9 Å. The second trace (dotted line) included the entire emission within the MLM bandpass, namely, the strong resonant lines of Mo^{23+} - Mo^{25+} and the quasi-continuum. The GIS trace should be identical to the MLM time history if the response of the instruments was as expected, and the agreement was excellent. The third time history (dashed line) included only the strong resonant lines of Mo^{23+} - Mo^{25+}. The difference between the two GIS traces (dotted and dashed lines) illustrated the large contribution of the quasi-continuum states to the total emission in this region. This contribution in the MLM and GIS time histories was ~30% for ohmically heated plasmas and ~50% for ICRF heated plasmas. The low resolution MLM spectrum between 65 - 80 Å (Fig. 6a) taken during a diverted ohmically heated plasma was fit as described in the previous section after a correction for the quasi-continuum contribution was applied.

The overall agreement between the GIS and the MLM spectral line brightnesses was reasonably good. For most of the lines the differences between the two measurements of the line brightnesses were less than 25%. The discrepancies in the MLM spectral fit of any individual line resulted from the error in fitting lines that were closer together in wavelength than the bandpass of the MLM. The agreement between the synthetic spectrum of the Mo^{23+} to Mo^{25+} charge states was also in fair agreement with the experimental spectrum. Even in this complex wavelength range a realistic and meaningful spectrum and time history were measured by the MLM-based polychromator. With more extensive atomic physics modeling of this wavelength region, the contribution of the quasi-continuum states to the total emission could have been determined theoretically, and the assistance of the GIS would have been unnecessary.

(c) The 30 - 45 Å Spectral Region of Carbon and Molybdenum:

At the highest resolution of the MLM ($\lambda \sim 0.5$ Å) which occurs at the lowest wavelength, the interpretation of the spectrum was not complicated. Here, the dominant emission was carbon, and its behavior in tokamaks is well understood. The carbon charge states exist near the edge of the plasma just inside the last closed flux surface (LCFS) for the central electron temperatures greater than 1 - 2 keV seen in the Alcator C-Mod Tokamak. The measured carbon spectrum from the MLM was very simple in the 30 - 40 Å region as is shown in Fig. 7(a). The four strong lines of interest seen in the MLM spectra were the Ly_α of C^{5+} at 33.7 Å, the $2p^6$ - $2p^5 3d$ of Ar^{8+} at 41.45 Å, and the C^{4+} $1s^2$-1s2p transitions at 40.3 and 40.7

Å [17]. Both the Ly_α of C^{5+} and the C^{4+} $1s^2$ - 1s2p transitions were seen clearly above the background of the Mo^{14+} to Mo^{22+} 3d - 4p and 3d - 4f transitions[18]. Argon was puffed into the plasma to obtain ion temperature measurements from X-ray spectroscopy. The calibrated spectral fit is shown in Fig. 7(b). Even though the lines were separated by roughly the bandpass of the MLM, the fit to the MLM spectra resulted in a realistic line ratio for the two C^{4+} lines. The ratio of the C^{4+} lines indicated that they existed at a temperature of 125 to 175 eV which was indeed at the edge of the plasma. The MLM polychromator measured a very good spectrum of carbon and argon. In this wavelength region, the MLM brightnesses could not be directly compared with the brightness from the GIS because the GIS could measure these lines only in second order (Fig. 6(c)). This comparison would be useful for a verification but was unnecessary for the analysis of the carbon spectrum from the plasma.

Atomic Physics Model:

Molybdenum:

The atomic physics model used to determine the impurity concentrations and the power losses through line emission consisted of the Multiple Ionization State Transport (MIST) [19] code and a collisional radiative model. MIST is a one dimensional (radial in cylindrical coordinates), time dependent impurity transport code which treats the ionization/recombination physics and the trace impurity particle transport simultaneously. Input into MIST were the experimentally measured radial

electron temperature, electron density, (Fig. 8) and dominant neutral impurity concentration. The trace impurity anomalous diffusive transport coefficients were determined from impurity injection experiments using the laser ablation technique [7]. MIST was run in the time independent mode and calculated the impurity charge state distributions in the plasma.

The original charge state distributions computed by MIST were found to describe inadequately the experimentally measured ion distributions of Mo^{23+} - Mo^{32+} measured in the Alcator C-Mod Tokamak plasma. The complexity of the atomic structure of the molybdenum ion has made difficult previous detailed computations of the ionization and recombination rates. The original ionization balance in MIST included collisional ionization rates from the ground state but not excitation-autoionization rates. The original recombination processes included were both radiative and dielectronic, the latter being approximated by the formula by Burgess-Mertz [20,21,22]. To improve the existing rates in the MIST, *ab initio* calculations were performed to produce accurate electron impact excitation, excitation-autoionization, and dielectronic recombination rates for molybdenum [23]. The radiative recombination and dielectronic recombination rates for Mo^{24+} - Mo^{39+} were obtained in the zero-density limit. Also, the excitation-autoionization rates have been calculated for Mo^{23+} - Mo^{32+}. Excitation-autoionization rates from the work by Mitnik [24] were included for the Cu like to Kr like (Mo^{6+} to Mo^{13+}) ions. The rates for the remaining ionization states were unaltered. The rates for Mo^{23+} - Mo^{32+} were verified experimentally on the Alcator C-Mod Tokamak by comparing the measured charge state distributions from VUV and X-ray spectrometers with those predicted by these calculations [25].

With this new ionization balance model and electron-impact excitation rates, the proper characterization of the molybdenum concentration and behavior in the plasma could be done.

A collisional radiative model was used to determine the emissivity for the transitions of the Mo^{14+} - Mo^{39+} ionization states. The electron collisional excitation rates and energy levels used in the CR model were calculated using the atomic physics package HULLAC [26,27,28]. Approximately 70000 transitions and experimental wavelengths for the resonant lines of interest were incorporated into the CR model. These included transitions from levels n = 2, 3 and 4 for Mo^{29+} to Mo^{39+}, n = 3, 4 for Mo^{14+} to Mo^{28+}.

The emissivity of each line was determined for each radial magnetic flux surface of the plasma. The flux surfaces were calculated using the magnetic flux surface reconstruction code EFIT [29]. The flux surfaces used in the MIST were on a grid of 50 points between r/a = 0 to 1.1 separated equally in radius. These emissivities were summed over the line of sight of the MLM-based polychromator to produce a synthetic spectrum of the plasma.

Carbon:

For carbon, the relatively simple ionic structure and the availability of experimentally established rate coefficients for the various atomic processes presented a much easier investigation of its behavior [30] in the high temperature low density tokamak plasmas. The ionization balance is well understood and, therefore, the ionization physics in MIST was considered accurate and was used without modification. The electron collision impact excitation rates for the C^{5+} Ly_α at 33.7 Å and the C^{4+} 1s-2p lines at 40.3 and 40.7 Å were those computed by Itikawa [31].

The contribution of molybdenum and carbon to the core value of Z_{eff} -1 for the plasma was determined from the atomic physics model using the equation:

$$(1)\quad Z_{eff} - 1 = \frac{\sum_{j}^{All\ ions} Z_j^2 n_j}{\sum_{j}^{All\ ions} Z_j n_j} - 1 = \frac{Z_{Mo}\left(Z_{Mo}-1\right)n_{Mo}}{n_e} + \frac{Z_C\left(Z_C-1\right)n_C}{n_e}$$

The first and second terms were the contribution to the Z_{eff} of molybdenum and carbon, respectively. Where Z was the ionization state of the impurity (Z was typically 33 for molybdenum in the core and Z was 6 for carbon), and n_{Mo} and n_C were the central molybdenum and carbon impurity densities from the atomic physics model.

Impurity Transport and Concentrations:

The spectra measured by the MLM-based polychromator and the synthetic spectra from the atomic physics model were compared to characterize the impurity behavior in an ohmically heated diverted plasma. A brightness from a single resonant line and the synthetic spectra can be used to yield impurity concentrations, contributions to Z_{eff} -1 and power loss information from a plasma using known transport coefficients. This could have been the approach taken. Instead, the ability of this multilayer mirror diagnostic to determine both the impurity concentration and the anomalous transport of impurities was explored using both the 60 - 85 Å and the 110 - 140 Å spectral regions. To determine the particle confinement time and the plasma transport of impurities, a laser ablation of molybdenum was introduced in to the plasma [32]. The time history of the Mo^{31+} 127.9 Å emission line was monitored by the MLM-based polychromator. The transport coefficients were determined for the impurity charge state distributions formed after the laser ablation. Although, the impurity charge state distributions that existed before the laser ablation were very similar to those formed after since these ablations did not perturb the plasma. The measured confinement time, τ, from the impurity ablation was ~ 22 ms. and was related to the diffusion coefficients, D, by [33]:

$$(2) \qquad \tau = \left(\frac{a^2}{D\, k^2} \right) \qquad V_C = 0$$

The variable, a, was the tokamak minor radius (~ 22 cm), and k (~ 2.405) was the first zero of the zeroth-order Bessel function. V_C is the anomalous convection velocity. Eq. 2 determined the central (r/a < 0.4) anomalous diffusion coefficient. The difference between the measured and the synthetic spectra in both the 60 - 85 Å and the 110 - 140 Å regions was minimized by adjusting the molybdenum concentration and the diffusion coefficient for 0.4 < r/a < 0.9. The resulting anomalous diffusion coefficient was 0.5 m^2/s for 0.0 < r/a < 0.9. The diffusion coefficient was set to 0.05 m^2/s at r/a = 1.0 with a linear interpolation to r/a = 0.9 [34]. No anomalous convection was needed. The convection velocities were explicitly set to zero. Neoclassical transport was not included in the analysis since the impurity behavior of the plasma can not be described correctly with neoclassical theory. The impurity transport of Alcator has been thoroughly investigated elsewhere [34]. The resulting molybdenum charge state distributions of interest predicted by the MIST are presented in Fig. 9. The individual emission lines predicted by the CR model are over-plotted in Fig. 2(b) and 6(b) with the GIS and MLM-based spectra. The synthetic spectrum was also degraded to the MLM resolution and directly compared with the total MLM-based polychromator brightness (Table II). The agreement was quite good. An intrinsic central molybdenum concentration in the plasma of ~ 1.2×10^{10} cm^{-3} resulted. The contribution to the average Z_{eff} -1 was ~ 0.11 of the measured value of ~ 0.8.

The anomalous transport in the plasma directly affects both the radial positions and the relative widths of the emission shells of molybdenum and carbon in the plasma and thus the brightness of the measured lines. The present analysis of the trace impurity transport was

possible due to the different radial positions of the emitting shells of Mo^{31+} and Mo^{23+} - Mo^{25+}. If the studied lines were emitted from shells that exist near the same radial position in the plasma (~ 1 cm apart), transport would not significantly alter their relative radial positions or widths and would not change the observed line brightnesses. Thus, any discrepancies in the brightness cannot be attributed to transport but only by problems in the atomic physics model. Hence, the line brightness measurements of charge states with emission shells at different plasma radii and together with an adequate physics model allowed the valid measurement of plasma transport parameters.

The carbon impurity concentrations and power losses were determined from the 30 - 50 Å spectra using the atomic physics model. For carbon, the spectrum of the three carbon lines was compared with the synthetic spectrum by only varying the carbon impurity concentration since the particle transport had been determined. The carbon charge state distribution predicted by MIST is plotted in Fig. 10. The resulting synthetic spectrum agreed quite well with the experimentally measured one (Table III, Fig. 7). The resulting calculated impurity concentration was 1.7×10^{12} cm^{-3}, two orders of magnitude greater than the measured molybdenum concentration. The carbon contributed a very significant 0.5 to the Z_{eff} -1 of 0.8.

Including the molybdenum and carbon impurity concentrations to the plasma, the Z_{eff} - 1 predicted by the model was ~0.61 of the measured 0.8. These two elements made up the majority of the trace impurities in the Alcator C-Mod Tokamak plasma. The remainder of the impurities were attributed to the other light impurities, such as oxygen and nitrogen.

These impurity measurements were performed during the initial operations of the Alcator C-Mod Tokamak. Therefore, the plasmas presented in this paper were dirtier, and the impurity concentrations were higher than are presently observed. The molybdenum concentration over time has remained unchanged for unboronized plasmas, but the carbon concentration has dropped by approximately an order of magnitude with a corresponding decrease in the Z_{eff}. With boronization, these impurity levels have dropped even further. In the plasmas presented in this paper, the calculated Z_{eff} from the MLM-based Polychromator and the atomic physics model was very consistent with the Z_{eff} measurement of the core plasma. This low resolution system and atomic physics model were capable of determining the dominant impurities in the plasma and predicting accurate and reliable Z_{eff} values.

Radiative Losses and Cooling Rate:

The complexity of the molybdenum ion atomic structure required a detailed investigation of the power radiated through line emission. To help cope with this complexity, two different methods were investigated for computing the radiated power. The electron temperature range examined was that of interest for the Alcator C-Mod Tokamak and was 0.05 to 10 keV. The first method involved the radiative cooling rate curve based on the work of Post and his use of the average ion model [35] (Fig. 11). This cooling rate curve did not explicitly include any ionization balance calculations, but instead assumed the presence of a single fictitious "average ion". This average ion had a single Z at a given temperature. The cooling

rate curve from the model was calculated in the coronal limit. The second method, designated hereafter as the spectral line model, involved the summation of the total radiation from our physics model at each temperature. The power radiated included both spectral line radiation and contributions from radiative recombination dielectronic recombination and bremstraalung. To calculate the line power contribution to the total cooling rate (dotted line), the total emissivity from each ionization state (Mo^{14+} to Mo^{39+}) was summed and then divided by both the electron and the molybdenum ion concentrations. The dashed-dot line included the contribution from both spectral line radiation, the recombination effects and bremstraalung. The formula recommended by Post for the radiative and dielectronic recombination power was used, but the *ab initio* data from the HULLAC package was substituted for the rate coefficients and the atomic structure levels. The recombination effects were only significant at electron temperatures greater than 1 keV. The two methods were in fair agreement, although the Post calculations will yield a larger radiated loss from molybdenum ions. The details of the cooling curve as well as comparisons with bolometery are discussed elsewhere [36].

These two methods were used to estimate the contribution of the total radiative losses from molybdenum for our experimental plasmas. These radiative losses were estimated to be ~ 170 kW from the spectral line model and ~ 230 kW from the Post cooling rate curve. They differ by about 50 %. The calculation from spectral line model yielded a better estimate of the total radiative losses from the plasma by molybdenum ions since the calculation from HULLAC are *Ab Initio*. The average ion model overestimated the total radiation from molybdenum. The total radiated

power measured by the bolometric system was measured to be ~ 450 kW. The results from both cooling curves indicated that a significant fraction of the radiative losses were from molybdenum ions. Molybdenum ions must emit most of the power from impurities since they were the only high-Z impurity in the plasma as confirmed by the GIS.

The radiated power calculations for carbon were straightforward due to the simplicity of the atomic structure of the carbon ion. Again, both the spectral line model and the Post work were examined. The comparison of the total radiated power predicted by Post was within 10% of the radiated power from the three carbon transitions included in the spectral line model. The predicted radiated power from the plasma was 40 - 50 kW. The Post work was an adequate means to predict radiative losses from the line emission of carbon. The radiation from carbon was a factor of 10 times less than the radiation from molybdenum. Note however, the radiation from molybdenum originated from a concentration 100 times smaller than that of carbon. The need to monitor even the small amounts high-Z impurity such as molybdenum in the plasma was found to be very important.

The total radiated power from the carbon and molybdenum impurities was ~ 210 kW as computed by the spectral line model and ~ 280 kW as computed by the Post model. The emission from these two dominant impurities accounted for 45 - 60% of the total radiated power measured by bolometery. The rest of the emitted radiation was assumed to be from nitrogen, oxygen, and neutral particles. The MLM-based polychromator and the atomic physics model could account for a significant fraction of the radiated power.

Conclusions:

An MLM-based polychromator has been installed on the Alcator C-Mod Tokamak to monitor the XUV spectroscopic emission of impurities in the plasma. The polychromator was a compact high-throughput device that could be used on future fusion physics devices such as ITER. Although the spectral resolution was lower ($\Delta\lambda \sim 7$ Å at $\lambda = 128$) than conventional VUV grating spectrometers, it was possible to extract meaningful information about impurity concentration and radiative losses in the plasma. The high resolution of grating instruments was not a necessity. With the proper choice of the spectral region and the use of an adequate atomic physics model, the MLM-based polychromator can be used for impurity analysis. For the specific case of the Alcator C-Mod Tokamak, the major impurities in this unboronized plasmas were molybdenum and carbon. The molybdenum ion concentration in the plasma was of great concern since all of C-Mod's plasma facing components were molybdenum blocks.

Estimates of molybdenum and carbon concentrations and power losses have been obtained from strong Mo^{23+} - Mo^{25+}, Mo^{31+}, C^{5+}, and C^{4+} emission lines recorded by the MLM-based polychromator, the MIST transport code and a detailed collisional radiative model. The physics models used up to date ionization, recombination, and excitation rates for molybdenum. The resulting molybdenum and carbon concentration have been found to be ~1.2×10^{10} cm^{-3} and ~1.7×10^{12} cm^{-3}, respectively. The total estimated contribution of both carbon and molybdenum to the measured Z_{eff} -1 of 0.8 was ~ 0.61. The total line power was estimated to be ~ 210 kW, which was less than the 280 kW predicted by the Post model. The

molybdenum and carbon impurity analysis from the spectral line model accounted for 45 - 60 % of the total radiative losses measured by the bolometric systems.

Acknowledgments:

The authors would like to thank the entire Alcator C-Mod staff for their expert operation of the tokamak and the use of their facility. We also thank the Princeton Plasma Physics Laboratory for use of the MIST transport code. This work was supported by U.S. DoE Grant DE-FG02-86ER53214 at JHU, Contract no. W-7405-ENG-48 at LLNL, and Contract No. DE-AC02-78ET51013 at MIT.

Plasma Current (kA)	800
Magnetic Field (T)	5.3
Major Radius (cm)	67
Minor Radius (cm)	22
Central Electron Density (cm^{-3}):	$1.2x10^{14}$
Central Electron Temperature (keV)	1.5
Measured Z_{eff} -1	0.8
Ohmic Input Power (kW)	860.
Total Radiated Power measured by Bolometer (kW)	450.

Table I: Plasma parameters of the Alcator C-Mod Tokamak during these experiments.

MLM-Based Polychromator Brightness at 127.9 Å (photons/sec/sr/cm^2)	$5.3x10^{14}$
Brightness predicted by model at 127.9 Å (photons/sec/sr/cm^2)	$5.4x10^{14}$
MLM-Based Polychromator Brightness at 74.9 Å (photons/sec/sr/cm^2)	$3.2x10^{14}$
Brightness predicted by model at 74.9 Å (photons/sec/sr/cm^2)	$3.2x10^{14}$
Power Radiated by Plasma from Molybdenum (Post) (kW)	230.
Power Radiated by Plasma from Molybdenum (Spectral Line Model) (kW)	170.
Contribution to Z_{eff} -1	0.11
Central Molybdenum Impurity Density (cm^{-3})	$1.2x10^{10}$

Table II: Experimental molybdenum line brightnesses, and the resulting molybdenum concentration and power losses as calculated by the atomic physics model and normalized to the Mo^{31+} 127.9 Å emission line.

MLM-Based Polychromator Brightness at 33.7 Å (photons/sec/sr/cm^2)	$1.2x10^{15}$
Brightness predicted by model at 33.7 Å (photons/sec/sr/cm^2)	$1.3x10^{15}$
MLM-Based Polychromator Brightness at 40.3 Å (photons/sec/sr/cm^2)	$4.3x10^{14}$
Brightness predicted by model at 40.3 Å(photons/sec/sr/cm^2)	$4.2x10^{14}$
Power Radiated by Plasma from Carbon (Post) (kW)	45.0
Power Radiated by Plasma from Carbon (Spectral Line Model) (kW)	41.0
Contribution to Z_{eff} -1	0.5
Central Carbon Impurity Density (cm^{-3})	$1.7x10^{12}$

Table III: Experimental carbon line brightnesses, and the resulting carbon concentration and power losses as calculated by the atomic physics model.

References:

[1] Regan, S.P., Finkenthal. M., May, M.J., Moos, H.W., Rev. Sci. Instrum., Vol. 66, No. 1, (1995) 770.

[2] May, M.J., Zwicker, A.P., Moos, H.W., Finkenthal, M., Terry, J.L., Rev. Sci. Instrum. Vol. 63, No. 10, (1992), p 5176.

[3] Meade, D.M., Nucl. Fusion, Vol. 14, 289 (1974).

[4] Content, D.A., Moos, H.W., Perry, M.E., et al., Nuc. Fusion, Vol. 30, No. 4, 707 (1990).

[5] Hsu, T.C., et al., Proc. 8th Joint Workshop on ECE and ECRH, IPP III/186, 409 (1993).

[6] Irby, J.H. et al., Rev. Sci. Instrum., Vol. 59, 1568 (1988).

[7] Graf, M.A., Rice, J.E., Terry, J.L, Marmar, E.S., Goetz, J.A., McCracken, G.M., Bombarda, F., May, M.J., Rev. Sci. Instrum. 66 (1) (1994) 636.

[8] Goetz, J.A. Lipschultz, B., Graf, M.A,. Kurz, C., Nachtrieb, R., Snipes, J.A., and Terry, J.L., J. Nucl. Mater., Vol. 220-222, (1995) 971-5.

[9] Ford, M.E., Marmar, E.S., Nuclear Fusion, Vol. 25, No. 2, 197-202 (1985).

[10] May, M.J., Finkenthal M., Regan S.P., Moos H.W., Terry J.L., Graf M.A., Fournier K., and Goldstein W.L., Rev. Sci. Instrum. 66 (1) January (1995) 561.

[11] Moos, H. W., Zwicker, A. P., Regan, S. P., and Finkenthal, M., RSI, Vol. 61, No. 10 (Part II), Oct. 1990, 2733-2737.

[12] Mansfield, M. W. D., Peacock, N. J., Smith, C. C., Hobby, M. G., and

Cowan, R. D., J. Phys. B, Vol 11, (1978) 1512.

[13] Sugar, J., Kaufman, V., et al., Journal of the Optical Society of America B, Vol. 4, No. 12, (1987) 1927.

[14] Kaufman, V., Sugar, J., Journal of the Optical Society of America B, Vol. 6, No. 2, (1989) 142.

[15] Kaufman, V., Sugar, J., Journal of the Optical Society of America B, Vol. 6, No. 8, (1989) 1444.

[16] Bauche, J., et al., Advances in Atomic and Molecular Physics, Vol. 23, 131 (1988).

[17] Kelly, R.L., Journal of Physical and Chemical Reference Data, Vol. 16, 1987.

[18] Schwob, J.L., Klapish, M., Schweitzer, N., Finkenthal, M., Brenton, C., DeMichelis, C., Mattioli, M., Phys. Lett., Vol. 62A, No. 2, 85 (1977).

[19] Hulse, R.A., Nuclear Technology/Fusion, Vol. 3, 259 (Mar 1983).

[20] Burgess, A., Ap. J., Vol. 139, 766 (1964)

[21] Burgess, A., Ap. J., Vol. 141, 1588 (1965).

[22] Mertz A., Cowan, R., Magee, N., "Power Losses from an Optically Thin Iron Seeded Plasma," Los Alamos Scientific Laboratory Report, No. LA-6220-MS (1976).

[23] Fournier, K.B., Cohen, M., Goldstein, W.H., Osterheld, A.L, Finkenthal, M., May, M.J., Terry, J., Graf, M.A., and Rice, J., Phys. Rev. A, Vol. 54, No. 5, 3870-3884 (1996).

[24] Mitnik, D., Mandelbaum, P., Scwob, J.L., Bar-Shalom, A., Oreg, J., and Goldstein, W.H., Phys. Rev. A, Vol. 50, No. 6, 4911- 4929 (1994).

[25] Rice, J.E., Terry, J.L., Fournier, K.B., Graf, M.A., Finkenthal, M., May, M.J., Marmar, E.S., Goldstein, E.S., Hubbard, A. E., J. Phys. B: Mol. Opt. Phys. Vol. 29, 2191 (1995).

[26] Bar-Shalom, A., Klapisch, M., and Oreg, J., Phys. Rev. A., Vol. 38 (1988) 1773.

[27] Klapisch, M., Comput. Phys. Commun. Vol 2 (1971) 269.

[28] Klapisch, M., J. Opt. Soc. Am., Vol. 67 (1977) 148.

[29] Lao, L.L. et al., Nucl, Fusion, Vol. 25, 1611 (1985).

[30] Isler, R.C., Nuc. Fusion, Vol. 24, No. 12, 1599 (1984).

[31] Y. Itikawa, S. Hara, T. Kato, S. Nakazaki, M. S., Pindzola, D. H. Crandall, At. Data Nucl Data Tables, Vol. 33, No. 1, 149 (1985).

[32] Graf, M.A., Rice, J.E., Terry, J.L, Marmar, E.S., Goetz, J.A., McCracken, G.M., Bombarda, F., May, M.J., Rev. Sci. Instrum. 66 (1) (1994) 636.

[33] Seguin, F.H., Petrasso, R., and Marmar, E.S., Phys. Rev. Lett., Vol. 51, No. 6, 455-458 (1983).

[34] Rice, J.E. Terry, J.L., Goetz, J.A., et. al. "Impurity Transport in Alcator", submitted to Physics of Plasmas.

[35] Post, D.E., Jensen R.V., Tarter, C.B., Grasberger, W.H., and Lokke, W.A, At. Data Nucl Data Tables, Vol. 20, 397 (1977).

[36] Fournier, K.F., May, M.J., et. al., "Calculation of the Radiative Cooling Curve Coefficient for Molybdenum in a Low Density Plasma", submitted to Nuclear Fusion.

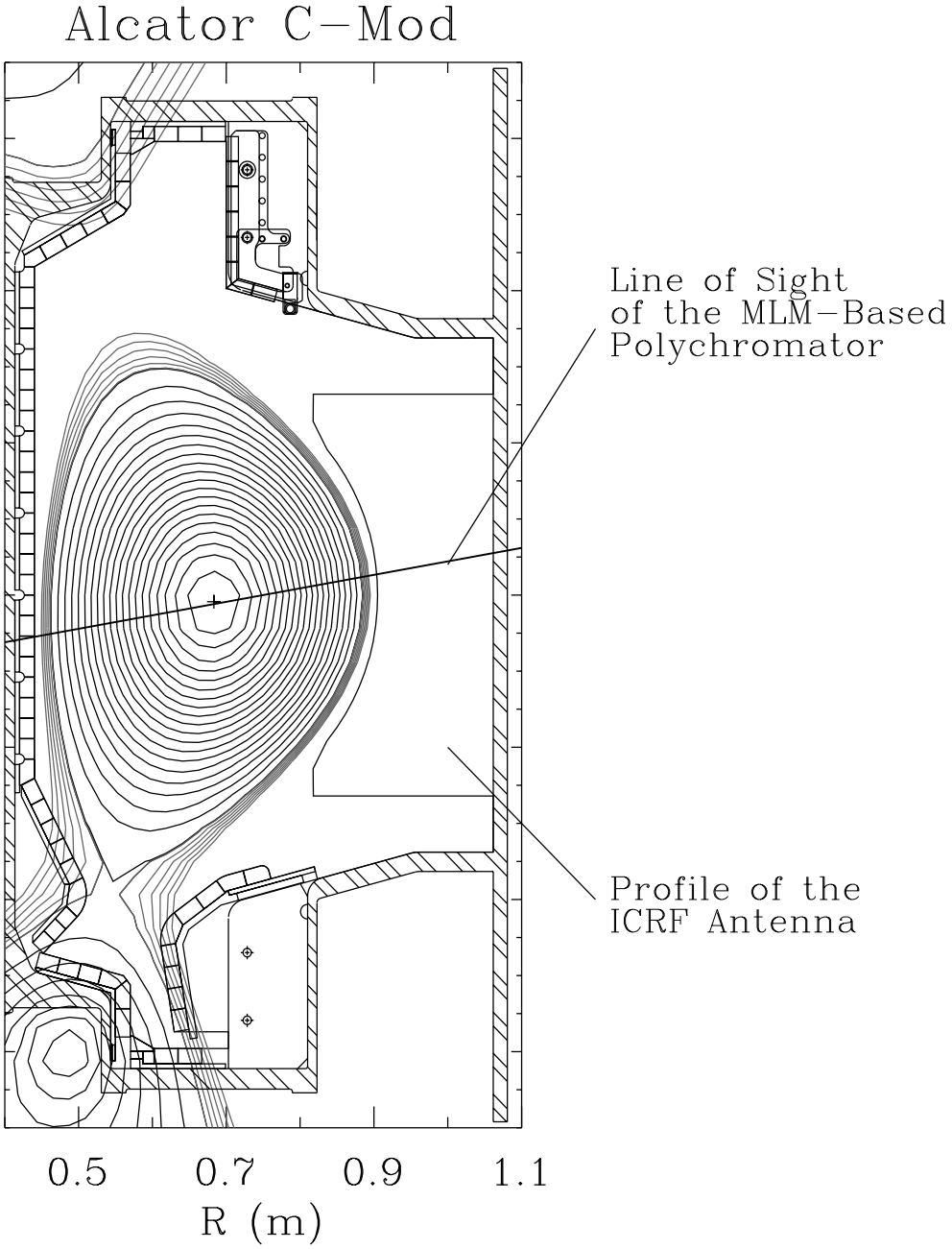

Fig. 1: Cross section of the Alcator C-Mod Tokamak plasma in a diverted configuration.

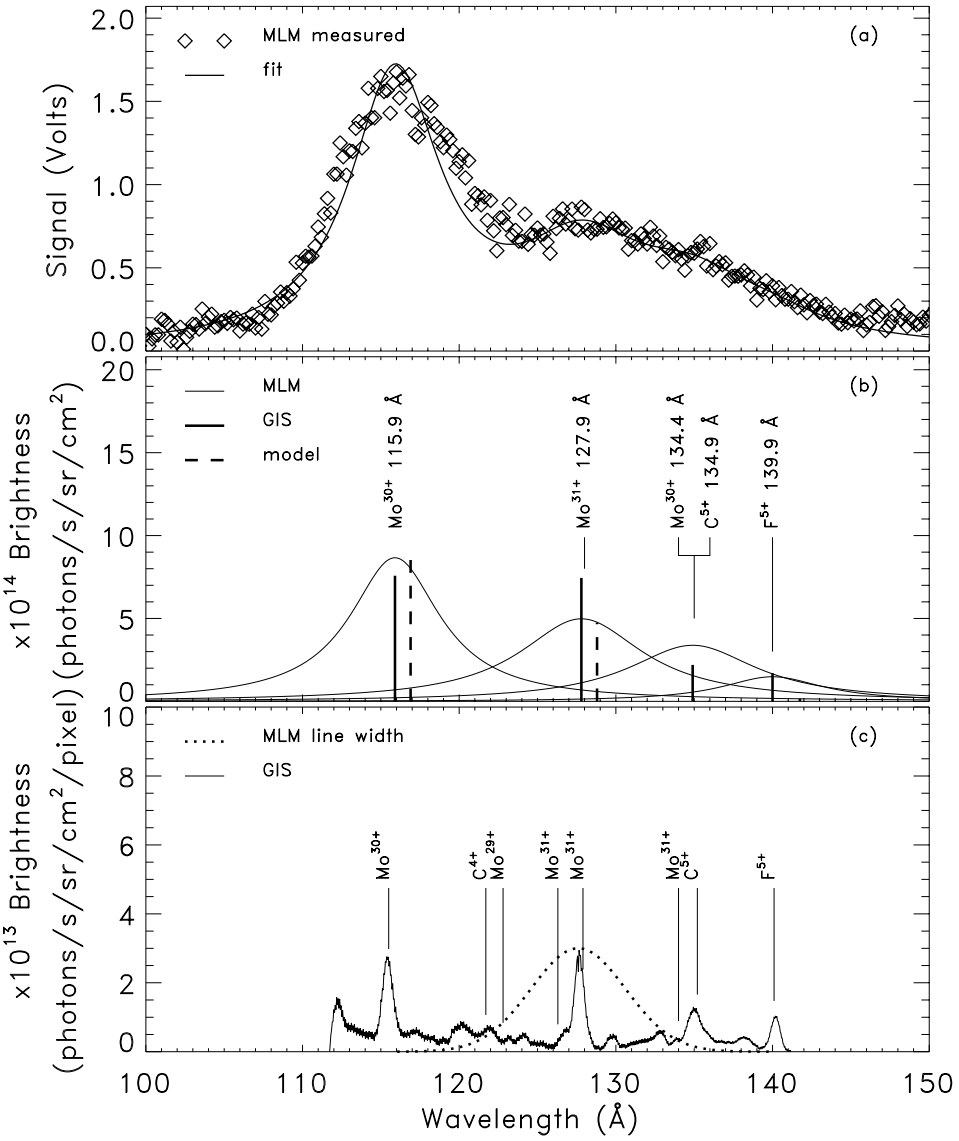

Fig. 2: (a) Uncalibrated spectrum from the MLM-based polychromator, (b) the photometrically calibrated spectral fit, the measured brightness from the grazing incidence spectrometer (GIS) and the modeled brightnesses, and (c) the GIS spectrum for Mo^{30+} and Mo^{31+} in the 100 - 150 Å range .

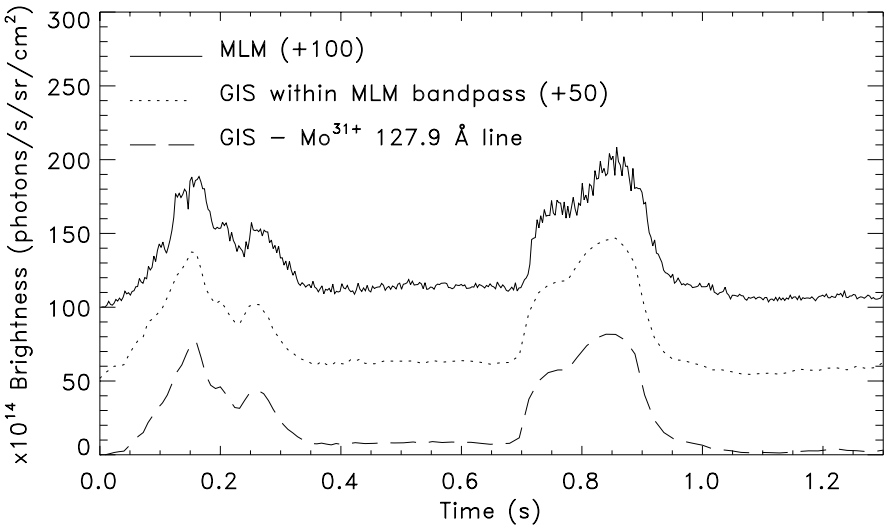

Fig. 3: Comparison of the time history of the grazing incidence spectrometer (GIS) for the Mo^{31+} emission line at 127.9 Å, the GIS signal within the bandpass of the MLM at 127.9 Å (offset +50 along y-axis for comparison), and of the MLM based-polychromator at 127.9 Å (offset +100 along y-axis for comparison).

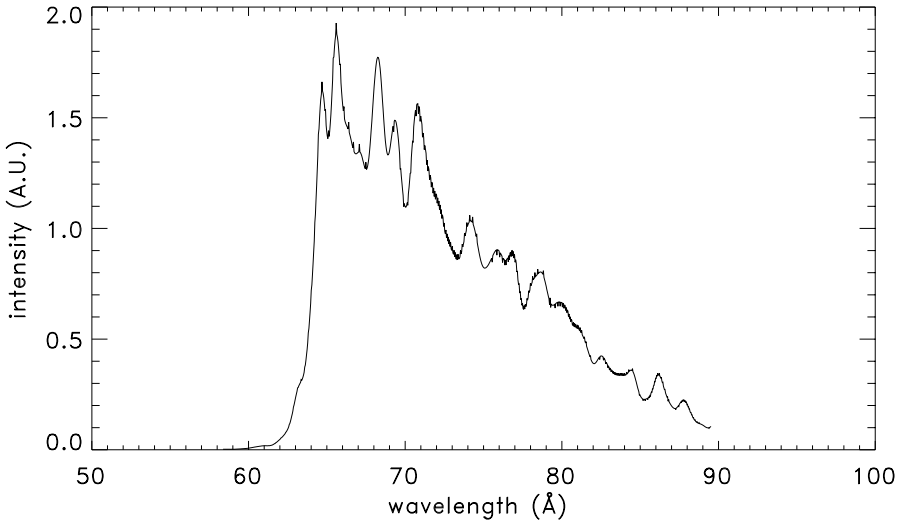

Fig. 4: Synthetic spectrum of the quasi-continuum of the Mo^{15+} - Mo^{22+} in the 60 - 85 Å range.

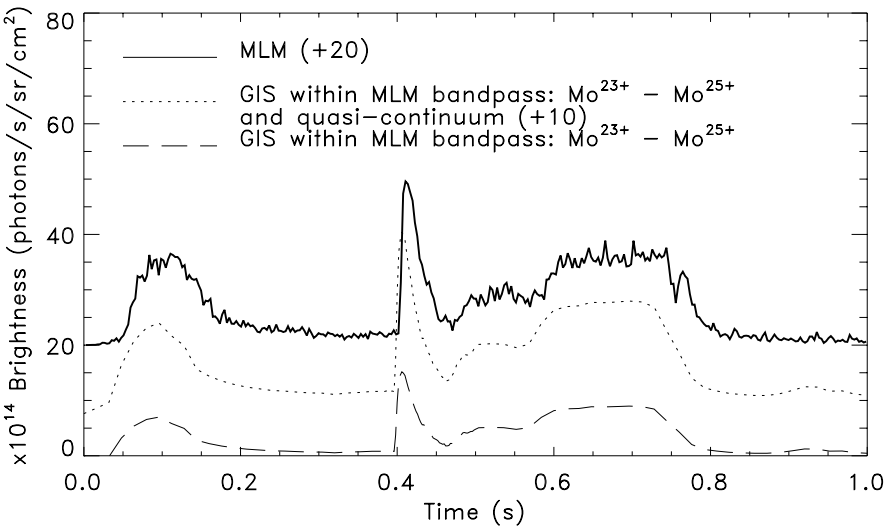

Fig. 5: Comparison of the time history of the grazing incidence spectrometer (GIS) for the Mo^{23+} - Mo^{25+} ionization states alone, the Mo^{23+} - Mo^{25+} ionization states with the unresolved transition arrays (offset +10 along y-axis for comparison), and of the MLM-based polychromator at 74.9 Å (offset +20 along y-axis for comparison).

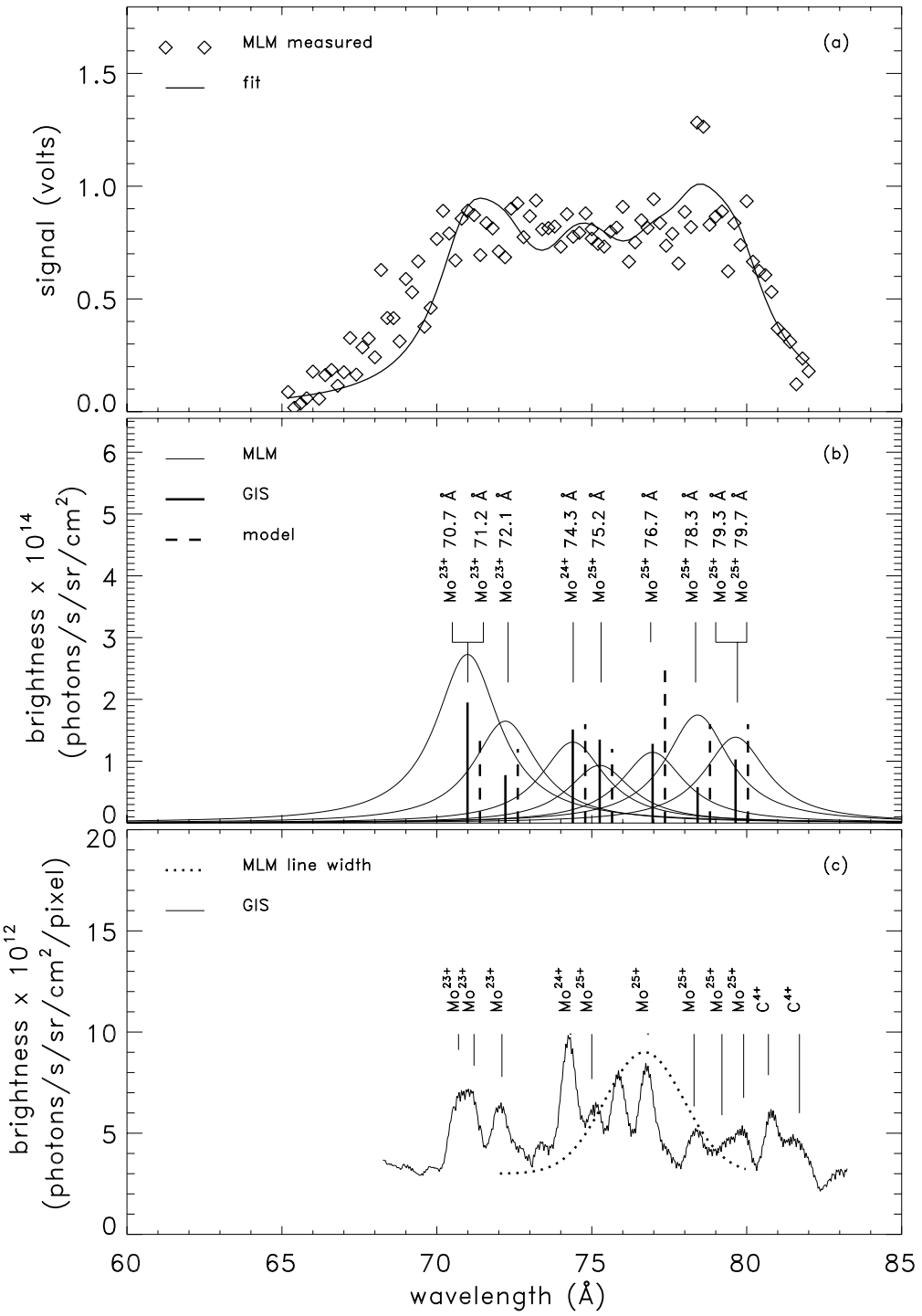

Fig. 6: (a) Uncalibrated spectrum from the MLM-based polychromator, (b) the photometrically calibrated spectral fit, the measured brightness from the grazing incidence spectrometer (GIS) and the modeled brightnesses, and (c) the GIS spectrum for Mo^{23+} to Mo^{25+} in the 60 - 85 Å range.

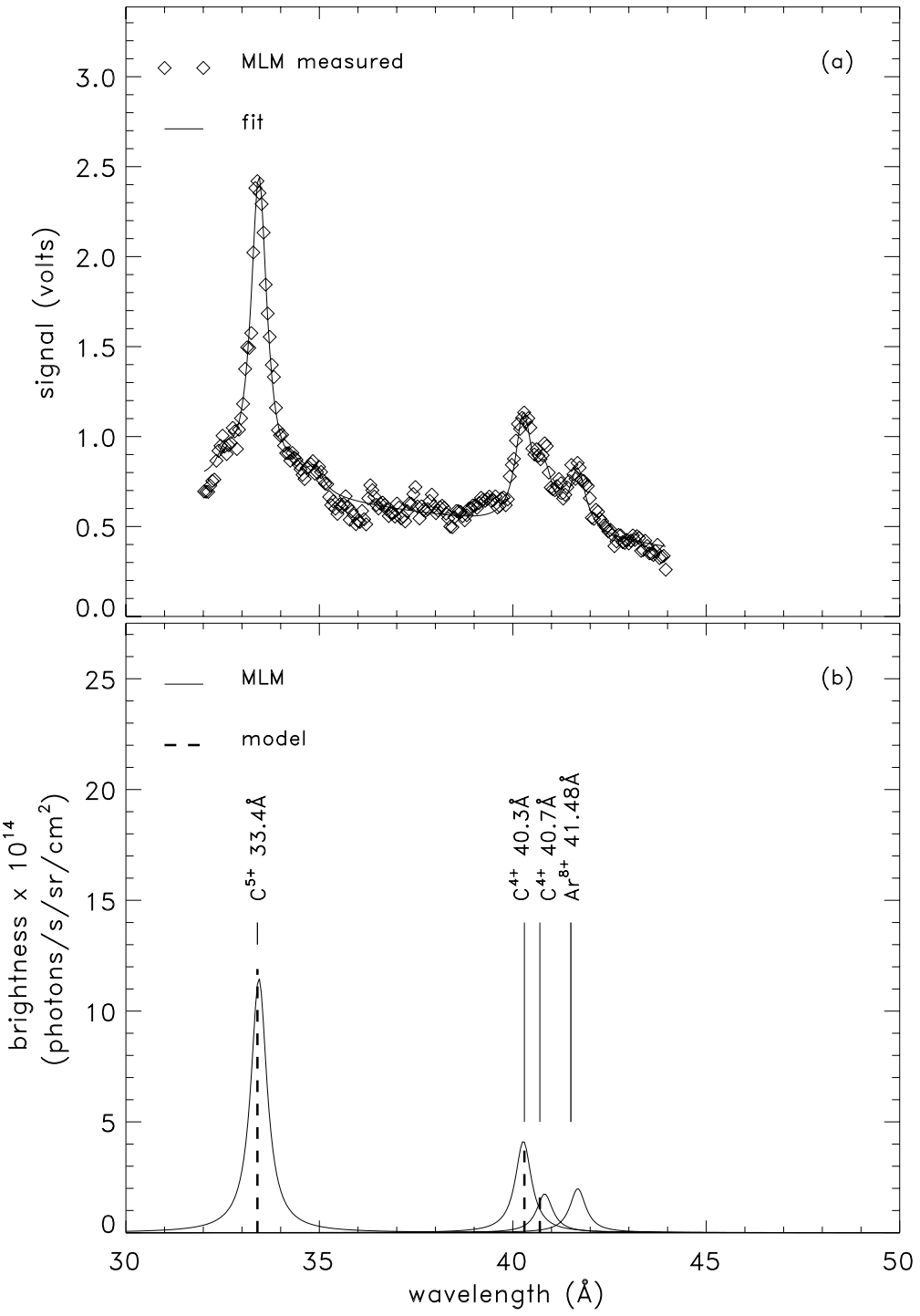

Fig. 7: (a) Uncalibrated spectrum from the MLM-based polychromator and the photometrically calibrated spectral fit and the modeled brightnesses (b) for the 30 - 40 Å range for C^{5+} and C^{4+}.

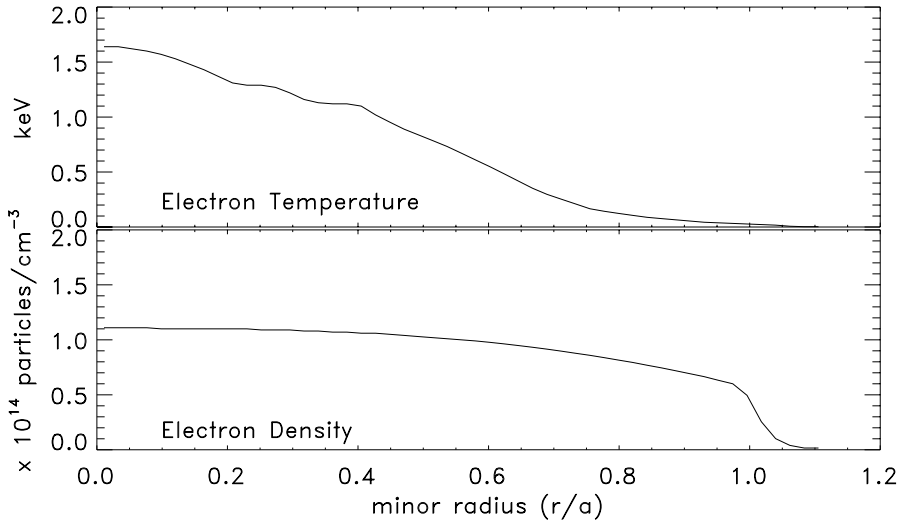

Fig. 8: Measured radial electron temperature and density profiles.

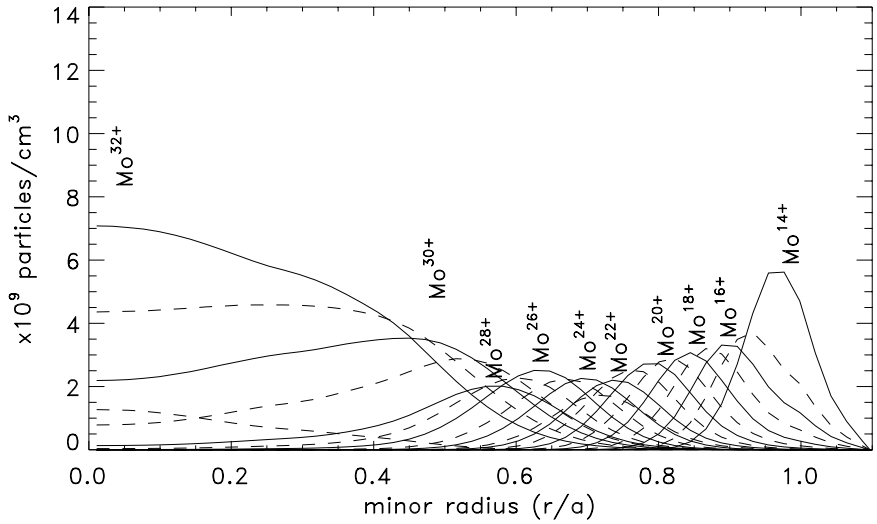

Fig. 9: Molybdenum charge state distribution calculated by MIST.

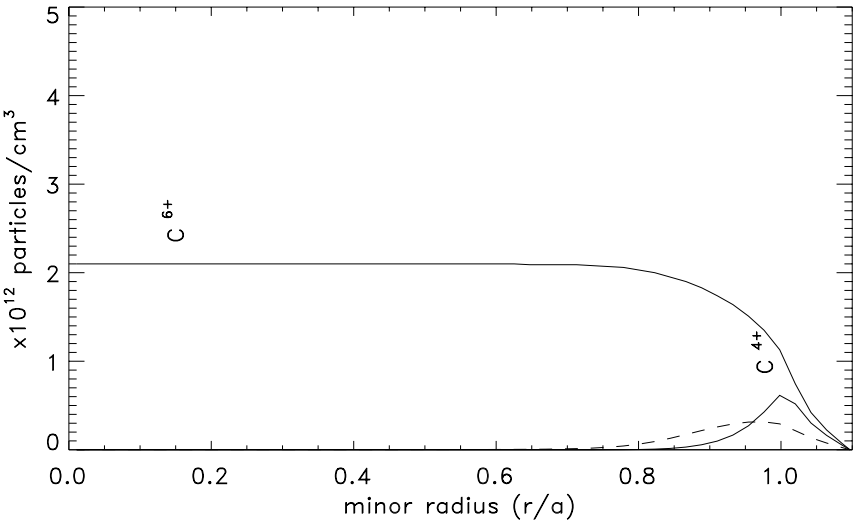

Fig. 10: Carbon charge state distribution calculated by MIST.

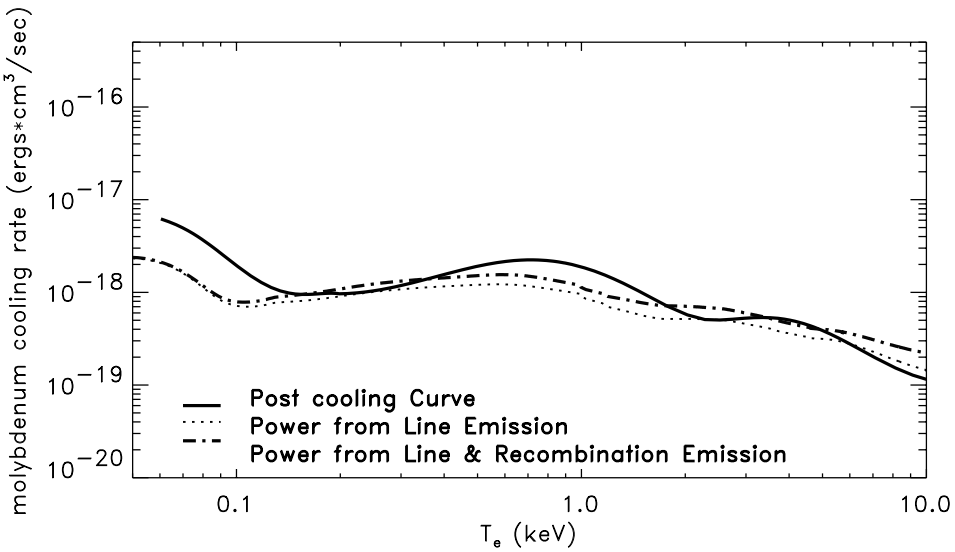

Fig. 11: The comparison between the cooling curves from the average ion model of Post and from the spectral line model.